Accessible phases via wave impedance engineering with *PT*-symmetric metamaterials

Sotiris Droulias,[1,2,*] Ioannis Katsantonis,[1,2] Maria Kafesaki,[1,2] Costas M. Soukoulis,[1,3] and Eleftherios N. Economou[1,4]

[1]*Institute of Electronic Structure and Laser, Foundation for Research and Technology Hellas, 71110 Heraklion, Crete, Greece*

[2]*Department of Materials Science and Technology, University of Crete, 71003 Heraklion, Greece*

[3]*Ames Laboratory and Department of Physics and Astronomy, Iowa State University, Ames, Iowa 50011, USA*

[4]*Department of Physics, University of Crete, 71003 Heraklion, Greece*

(Received 10 September 2019; published 22 November 2019)

Optical systems that respect parity-time (*PT*) symmetry can be realized with proper incorporation of gain/loss materials. However, due to the absence of magnetic response at optical frequencies, the wave impedance is defined entirely by their permittivity and, hence, the *PT*-symmetric character is controlled solely via their refractive index. Here, we show that the separate tuning of the wave impedance enabled by metamaterials can grant access to wide control of the exceptional points, appearance of mixed phases (coexistence of *PT*-symmetric and *PT*-broken phases) and occurrence of phase reentries, not easily realizable with natural materials.

DOI: 10.1103/PhysRevB.100.205133

I. INTRODUCTION

Optical systems with gain and loss that respect parity-time (*PT*) symmetry can have real eigenvalues despite their non-Hermitian character; the eigenvalues remain real below some critical value of the potential, the so-called exceptional point (EP), above which they become complex and hence the EP marks the passing from the *PT*-symmetric phase to the broken-*PT* phase. This is an idea, originally introduced in the context of quantum mechanics [1–4], which quickly found fertile ground in optics due to the mathematical equivalence with paraxial beam propagation, which is described by a Schrödinger-like equation [5–11]. The extension of *PT* symmetry to systems in which the eigenvalues refer to those of the scattering matrix [12–21] led to novel phenomena, such as coherent perfect absorption [13,14], the *PT*-laser absorber [15,16], and anisotropic transmission resonances [18]. In such systems, the condition to achieve *PT* symmetry is expressed in terms of the permittivity ε and permeability μ as $\varepsilon(\mathbf{r}) = \varepsilon^*(-\mathbf{r})$ and $\mu(\mathbf{r}) = \mu^*(-\mathbf{r})$, where $\mathbf{r}$ is the position operator and the asterisk denotes the complex conjugate [22,23]. When realized with natural optical materials, the magnetic response is absent and, therefore, the *PT* condition can be controlled only via ε. However, most recently, some works combined *PT* symmetry with metamaterials [22–27], which could extend these ideas to new limits, as metamaterials can be designed to have the desired ε and μ, at almost any frequency [28].

While the ability to control the *PT* phase can grant access to important properties, such as (a) mixed phases (coexistence of *PT*-symmetric and *PT*-broken phase) and (b) phase reentries (multiple passes among all possible phases), these aspects have not been investigated thoroughly. For example, in Ref. [29] the occurrence of mixed phases was shown to require polarization converting elements, while phase reentries were shown in [27] for TE waves in the special case of epsilon near-zero metamaterials only.

In this work, we show that the coexistence of *PT*-symmetric and *PT*-broken phases occurs naturally in systems as simple as a one-dimensional gain/loss bilayer. These mixed phases emerge in oblique incidence [30–32] as a result of the different wave impedances of TE and TM linearly polarized waves, which are otherwise identical in normal incidence and therefore in that case the mixed phase vanishes. By properly engineering the wave impedance, we show that the passing of TE waves from the *PT*-symmetric to the *PT*-broken phase can precede, succeed, or even coincide with that of the TM waves, thus allowing for tuning and eventually suppressing the mixed phase. We also show that, while natural materials favor a single exceptional point and thus a unique phase change, with metamaterials it is possible to engineer the wave impedance and observe multiple exceptional points and therefore phase reentries. Last, an important aspect of our work is the formulation in terms of the refractive index n and the wave impedance ζ. This approach provides a generalized description and deeper insight to the mechanism of phase change, as compared to all previous works where the analysis is based on ε and μ.

II. *PT*-SYMMETRIC GAIN/LOSS BILAYER

A. Conditions for *PT*-symmetric phase in TE and TM polarizations

Considering one-dimensional systems, the conditions to achieve *PT* symmetry for parameters changing, e.g., along the z direction are expressed in terms of the relative permittivity ε and relative permeability μ as $\varepsilon(z) = \varepsilon^*(-z)$ and $\mu(z) = \mu^*(-z)$ [22,23]. These impose on the refractive index $n = \sqrt{\varepsilon\mu}$ and the wave impedance $\zeta = \sqrt{\mu/\varepsilon}$ to fulfill

$$n(z) = n^*(-z), \quad \zeta(z) = \zeta^*(-z). \tag{1}$$

Such conditions can be satisfied in the system of Fig. 1, which consists of two homogeneous gain/loss slabs which are infinite on the xy plane and have finite length along the

*sdroulias@iesl.forth.gr

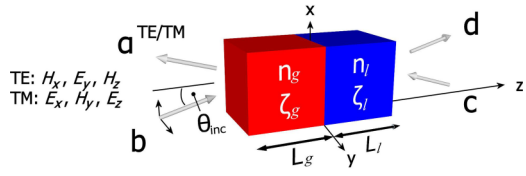

FIG. 1. A *PT*-symmetric heterostructure with a single gain/loss bilayer. The complex material parameters n_i, ζ_i are the refractive index and the wave impedance, respectively, and the subscript $i = \{g, l\}$ denotes whether they are located in the *gain* (red) or the *loss* (blue) region. For *PT* symmetry the shown parameters satisfy $n_g = n_l{}^*$, $\zeta_g = \zeta_l{}^*$, and $L_g = L_l$. The incident and scattered waves can be either TE or TM polarized, as shown.

z direction. Without loss of generality, gain (loss) is assumed to be embedded entirely in the left (right) slab.

To study the scattering properties of the gain/loss bilayer, we assume that waves arrive at angle ϑ_{inc} from either side of the system (propagating along the z direction) and we measure the scattered fields. The system is assumed to be in a homogeneous environment (air, for simplicity) and, hence, the waves exit the system at the same angle. Their polarization can be a mixture of TE components (H_x, E_y, H_z) and TM components (E_x, H_y, E_z) as shown in Fig. 1, where b, c, and a, d are the amplitudes of the incoming and outgoing waves, respectively. Although *PT*-symmetry requirements impose certain conditions in the loss and gain regions [see Eq. (1)], we start with slabs of arbitrary lengths, L_g, L_l and arbitrary material parameters n_g, n_l, ζ_g, ζ_l to obtain general expressions. Because the two polarization states are orthogonal to each other, the system can be described by two independent 2 $\times$ 2 scattering matrices, namely S^{TE} and S^{TM}, corresponding to TE and TM waves, respectively. Each individual S^p matrix [the superscript $p = \{\mathrm{TE}, \mathrm{TM}\}$ denotes the respective polarization] consists of two reflection and two transmission amplitudes, namely $r_L^p, r_R^p, t_L^p, t_R^p$, where the subscript L, R indicates incidence from "*Left*" or "*Right*," respectively (see Appendix for analytical expressions). As in the case of normal incidence [16,18], we find for both polarizations that $r_L^p \neq r_R^p$ and $t_L^p = t_R^p \equiv t^p$. In general, r_L^p, r_R^p, and t^p are different for TE and TM waves, except for normal incidence, where they become identical. Following the standard definition [16,18], S^p is written as

$$\begin{bmatrix} a \\ d \end{bmatrix} = S^p \begin{bmatrix} b \\ c \end{bmatrix} \equiv \begin{bmatrix} r_L^p & t^p \\ t^p & r_R^p \end{bmatrix} \begin{bmatrix} b \\ c \end{bmatrix}. \tag{2}$$

To identify whether the system lies in the *PT*-symmetric or *PT*-broken phase, we need to examine the eigenvalues $\lambda_{1,2}^p$ of S^p, $\lambda_{1,2}^p = [r_L^p + r_R^p \pm \sqrt{(r_L^p - r_R^p)^2 + 4(t^p)^2}]/2$ [18]. Because $r_L^{\mathrm{TE}} \neq r_L^{\mathrm{TM}}$, $r_R^{\mathrm{TE}} \neq r_R^{\mathrm{TM}}$, and $t^{\mathrm{TE}} \neq t^{\mathrm{TM}}$ in oblique incidence, the eigenvalues are different as well for each of the two polarizations. For each individual polarization, due to the presence of gain and loss, $|\lambda_{1,2}^p| \neq 1$ in general. However, if we apply *PT* conditions an exceptional point emerges, below which $|\lambda_1^p| = |\lambda_2^p| = 1$ (*PT*-symmetric phase), and λ_1^p, λ_2^p become an inverse conjugate pair above it, satisfying $|\lambda_1^p||\lambda_2^p| = 1$ [16,18] (*PT*-broken phase). As shown in Ref. [16], for the eigenvalues of S^p to satisfy $|\lambda_1^p| = |\lambda_2^p| = 1$ and therefore for the system to be in the *PT*-symmetric phase, the criterion is $|(r_L^p - r_R^p)/t^p| < 2$. For each of the two polarizations, after some calculations we find that this condition can be written as

$$\mathrm{TE}: \quad \left| \left(\frac{Z_l^{\mathrm{TE}}}{Z_g^{\mathrm{TE}}} - \frac{Z_g^{\mathrm{TE}}}{Z_l^{\mathrm{TE}}} \right) \sin(\delta_g) \sin(\delta_l) \right| < 2, \tag{3a}$$

$$\mathrm{TM}: \quad \left| \left(\frac{Z_l^{\mathrm{TM}}}{Z_g^{\mathrm{TM}}} - \frac{Z_g^{\mathrm{TM}}}{Z_l^{\mathrm{TM}}} \right) \sin(\delta_g) \sin(\delta_l) \right| < 2, \tag{3b}$$

where $Z_{g/l}^{\mathrm{TE}} = \frac{\zeta_{g/l}}{\cos\vartheta_{g/l}}$, $Z_{g/l}^{\mathrm{TM}} = \zeta_{g/l}\cos\vartheta_{g/l}$ is the wave impedance for TE and TM waves, respectively, and $\delta_{g/l} = n_{g/l}(\omega/c)L_{g/l}\cos\vartheta_{g/l}$ [$n_{g/l}, \zeta_{g/l}$ are defined according to Eq. (1)]. The angle $\vartheta_{g/l}$ is the wave-propagation angle inside the *g/l* region and is defined by the continuity of the tangential k components as $\sin(\vartheta_{inc}) = n_{g/l}\sin(\vartheta_{g/l})$ (the refractive index of the exterior—-air—-is unity). Equations 3(a) and 3(b) are the central results of this work, which we analyze next.

B. Mixed phases in natural nonmagnetic optical materials

With simple inspection, Eqs. (3a) and (3b) have the same general form, which is a consequence of the duality of Maxwell's equations for *E*- and *H*- fields; however, they are not identical. Due to the $\cos\vartheta_{g/l}$ term which appears asymmetrically in $Z_{g/l}^{\mathrm{TE}}, Z_{g/l}^{\mathrm{TM}}$, the term in parenthesis in the left-hand side of Eq. (3) is different among TE and TM waves and therefore the exceptional points for the two polarizations are spontaneously different. As a result, one polarization can pass to the *PT*-broken phase while the other still resides in the *PT*-symmetric phase, thus giving rise to a mixed *PT* phase for waves of arbitrary polarization, such as unpolarized light. The emergence of the mixed phase is thus a consequence of oblique incidence entirely, as for normal incidence where $\vartheta_{inc} = 0$ and therefore $\vartheta_g = \vartheta_l = 0$, Eqs. (3a) and (3b) become identical and therefore the exceptional points of both polarizations coincide, as shown in Eq. (4):

$$\underset{(\theta_{inc}=0)}{\mathrm{TE/TM}}: \left| \left(\frac{\zeta_l}{\zeta_g} - \frac{\zeta_g}{\zeta_l} \right) \sin\left(n_g \frac{\omega}{c} L_g \right) \sin\left(n_l \frac{\omega}{c} L_l \right) \right| < 2. \tag{4}$$

To demonstrate the above findings, we assume a nonmagnetic medium ($\mu_g = \mu_l = 1$) with $n_g = 2 - 0.2i$, $n_l = 2 + 0.2i$, as considered in previous works [18], and we scan the angle of incidence ϑ_{inc}. The two slabs have equal length $L_g = L_l \equiv L/2$ and for each ϑ_{inc} we calculate the eigenvalues of S^{TE}, S^{TM} as a function of the normalized frequency $\omega L/c$ (c is the vacuum speed of light). The cases where both polarizations are in the *PT*-symmetric or the *PT*-broken phase are denoted in Fig. 2(a) as "symmetric *PT*" and "broken *PT*," respectively. The region marked as "mixed *PT*" denotes that one polarization has passed into the broken-*PT* phase, while the other still resides in the *PT*-symmetric phase. In Fig. 2(b) we show explicitly the calculated eigenvalues for $\vartheta_{inc} = 30^\circ$ and $\vartheta_{inc} = 60^\circ$.

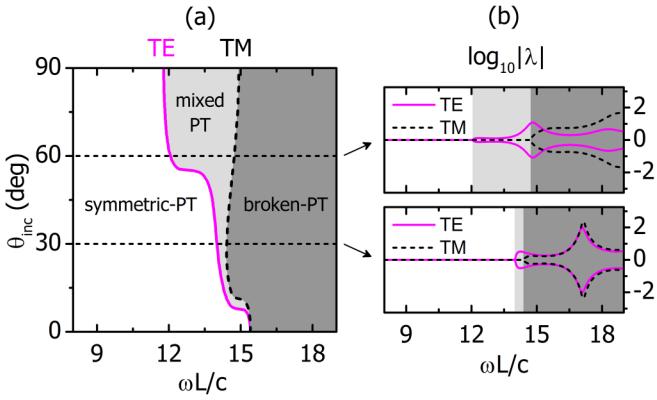

FIG. 2. Mixed phases as a consequence of oblique incidence, for a nonmagnetic medium ($\mu = 1$) with $n_{g/l} = 2 \mp 0.2i$. (a) Phase diagram and (b) calculated scattering matrix eigenvalues for $\vartheta_{inc} = 30^\circ$ and 60°. In the "symmetric-*PT*" and "broken-*PT*" regions both TE and TM polarizations are in the same phase. In the "mixed-*PT*" region TE waves have passed into the *PT*-broken phase, while TM waves still reside in the *PT*-symmetric phase.

C. Mixed phases and phase reentries in metamaterials

Clearly, the exceptional points for TE and TM waves split spontaneously when we depart from normal incidence, but, if desired, the mixed phase can be suppressed even in oblique incidence, with properly engineering the wave impedance. Such an extraordinary case, although difficult to observe with natural nonmagnetic optical materials, can be accomplished with metamaterials, which allow for tailored electric and magnetic response via their resonances. For example, the fishnet metamaterial, which provides simultaneously electric and magnetic response, could serve as a realistic system for tailoring the wave impedance [28]. To understand how, let us write the complex wave impedance for the gain and loss regions in polar form as $\zeta_g = |\zeta_g|\exp(i\varphi_g)$ and $\zeta_l = |\zeta_l|\exp(i\varphi_l)$, respectively. The *PT* conditions impose $|\zeta_g| = |\zeta_l| \equiv |\zeta|$ and $\varphi_g = -\varphi_l \equiv \varphi$, i.e., $\zeta_g = |\zeta|e^{+i\varphi}$ and $\zeta_l = |\zeta|e^{-i\varphi}$. Then, the magnitude $|\zeta|$ is eliminated everywhere in Eqs. (3a) and (3b) and terms of the form $e^{\pm 2i\varphi}$ appear, as shown in Eqs. (5a) and (5b):

$$\text{TE}: \quad \left| \left(e^{-2i\phi} \frac{\cos\theta_g}{\cos\theta_l} - e^{+2i\phi} \frac{\cos\theta_l}{\cos\theta_g} \right) \sin(\delta_g)\sin(\delta_l) \right| < 2, \tag{5a}$$

$$\text{TM}: \quad \left| \left(e^{-2i\phi} \frac{\cos\theta_l}{\cos\theta_g} - e^{+2i\phi} \frac{\cos\theta_g}{\cos\theta_l} \right) \sin(\delta_g)\sin(\delta_l) \right| < 2. \tag{5b}$$

This result implies that the positions of the exceptional points are not expected to depend on the magnitude of ζ, but solely on the relative strength between its real and imaginary part, which is expressed via φ. Simple observation leads to the conclusion that Eqs. (5a) and (5b) become identical if φ becomes multiples of $\pi/4$. This means that the exceptional points of TE and TM waves coincide if $|\mathrm{Re}(\zeta_{g/l})| = |\mathrm{Im}(\zeta_{g/l})|$ or $\mathrm{Re}(\zeta_{g/l}) = 0$ or $\mathrm{Im}(\zeta_{g/l}) = 0$ and this causes the mixed phases to vanish. Furthermore, a sign flip in φ interchanges Eqs. (5a) and (5b), i.e., the exceptional points of TE and TM waves exchange positions. From this analysis it is also evident that the refractive index does not participate in the tailoring of the mixed phases. This is not surprising, as n appears only in the arguments of the sine terms in Eqs. (5a) and (5b), which are identical for both expressions and, hence, the mixed phases are tailored via the wave impedance entirely. We note here that with natural gain/loss materials in which $\mu_g = \mu_l = 1 \rightarrow \zeta_{g/l} = (1/\varepsilon_{g/l})^{1/2} = 1/n_{g/l}$, and therefore $|\mathrm{Re}(\zeta_{g/l})|/|\mathrm{Im}(\zeta_{g/l})| = |\mathrm{Re}(n_{g/l})|/|\mathrm{Im}(n_{g/l})|$. Due to this result, because $|\mathrm{Re}(n_{g/l})| \gg |\mathrm{Im}(n_{g/l})|$ it follows that $|\mathrm{Re}(\zeta_{g/l})| \neq |\mathrm{Im}(\zeta_{g/l})|$ and, hence, the mixed phases appear naturally; to eliminate them, independent tuning of the wave impedance is required, i.e., a magnetic response is necessary.

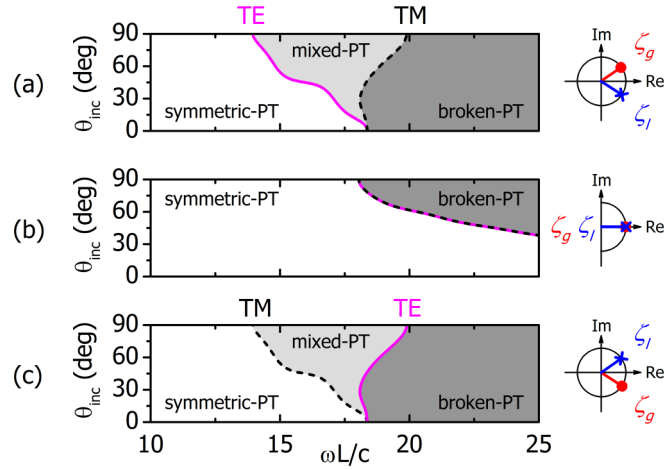

FIG. 3. Engineering of mixed phases via the wave impedance, $\zeta_{g/l} = |\zeta|e^{\pm i\varphi}$, for a system with $n_{g/l} = 2 \mp 0.2i$ and $|\zeta| = 0.5$. (a) $\varphi = +3^\circ$, (b) $\varphi = 0$, (c) $\varphi = -3^\circ$. The phase separation depends solely on φ (not on $|\zeta|$, which just adjusts the magnitude of the eigenvalues in the broken-*PT* phase). A sign flip in φ exchanges the position of the TE and TM exceptional points [compare (a), (c)] and for $\varphi = m \times \pi/4$ (m: integer) the mixed phase is completely suppressed, as shown in (b) for $m = 0$.

To demonstrate the above findings, we return to the system of the previous example with $n_g = 2 - 0.2i$, $n_l = 2 + 0.2i$, for which we now allow for magnetic response. We set $|\zeta| = 0.5(\sim |1/n_{g/l}|)$ and tune the wave impedance via the angle φ. Figure 3 shows examples for $\varphi = +3^\circ$ [panel (a)], $\varphi = 0$ [panel (b)], and $\varphi = -3^\circ$ [panel (c)]. As predicted, the phase separation does not depend on the magnitude of ζ, but solely on φ ($|\zeta|$ just adjusts the magnitude of the eigenvalues in the broken-*PT* phase and not the position of the exceptional point, see Appendix). A sign flip in φ exchanges the position of the TE and TM exceptional points [compare Figs. 3(a) and 3(c)] and for $\varphi = m \times \pi/4$ (m: integer) the mixed phase is completely suppressed as shown in (b), which corresponds to the case of $m = 0$.

Engineering the wave impedance with metamaterials can also grant access to phenomena not easily obtainable with natural materials, such as phase reentries, as a consequence of multiple exceptional points. To understand how this is possible, let us consider the case of normal incidence, for which Eq. (4) is simplified considerably and helps elucidate the important aspects. If we write the *PT*-symmetric n and ζ

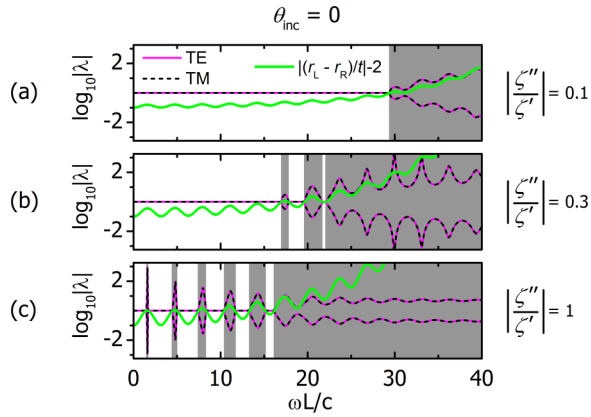

FIG. 4. Explanation of phase reentries via wave impedance engineering for a system with $n_{g/l} = 2 \mp 0.1i$ and $\zeta_{g/l} = \zeta' \pm i\zeta''$ (normal incidence). The ratio $|\zeta''/\zeta'|$ tunes the oscillation amplitude of the lhs of Eq. (6), plotted as green line. (a) Weak oscillation for $|\zeta''/\zeta'| = 0.1$ and single exceptional point. (b) Intermediate oscillation for $|\zeta''/\zeta'| = 0.3$ and initiation of phase reentries. (c) Strong oscillation for $|\zeta''/\zeta'| = 1$, leading to multiple phase reentries. For oblique incidence these results become richer, as mixed phases are introduced.

as $n_{g/l} = n' \mp in''$, $\zeta_{g/l} = \zeta' \pm i\zeta''$, Eq. (4) is now expressed in terms of the real quantities n', n'', ζ', ζ'' as

$$\underset{(\theta_{inc}=0)}{\text{TE/TM}} : \left| \frac{2i\zeta'\zeta''}{\zeta'^2 + \zeta''^2} \left(\cos\left(n' \frac{\omega L}{c} \right) - \cosh\left(n'' \frac{\omega L}{c} \right) \right) \right| < 2. \tag{6}$$

The left-hand side (lhs) of this inequality consists of an oscillatory part (cos term) with amplitude $2\zeta'\zeta''/(\zeta'^2 + \zeta''^2)$, which undergoes an exponentially growing offset (cosh term) with a rate that depends on the strength of n'', i.e., ζ tunes the oscillation amplitude, while n tunes its offset. Phase reentries mean that the lhs of Eq. (6) exceeds the right-hand side multiple times as function of $\omega L/c$. This requires strong oscillatory amplitude, which is maximized for $\zeta' = \pm\zeta''$, along with suspended offset, i.e., relatively weak n''. We note here that with natural gain/loss materials in which $\zeta_{g/l} = 1/n_{g/l}$, the oscillation amplitude becomes $2n'n''/(n'^2 + n''^2)$ and, hence, the need for strong oscillation amplitude is now expressed as $n'' = n'$, thereby contradicting the need for weak amplitude offset, i.e., $n'' \ll n'$. Because both requirements involve n'' in the opposite manner, it is somewhat difficult to achieve phase reentries with natural materials; however, with metamaterials, such cases are possible.

In Fig. 4 we show the eigenvalues for a system with $n' = 2$ and $n'' = 0.1$ (i.e., $n_{g/l} = 2 \mp 0.1i$) in normal incidence, for which $\zeta' = 1$, and ζ'' is tuned among three distinct values, namely 0.1, 0.3, and 1, in order to adjust the oscillation amplitude of the lhs of Eq. (6), which we plot in Fig. 4 as $|(r_L - r_R)/t| - 2$, where $r_L^p \equiv r_L$, $r_R^p \equiv r_R$, and $t^p \equiv t$ (due to normal incidence the scattering amplitudes are identical for both polarizations).

For $\zeta'' = 0.1$ (weak oscillation) the system passes on to the broken-PT phase at $\omega L/c = 29.4$. As ζ'' becomes stronger, the oscillation becomes stronger and for $\zeta'' = 0.3$ a double-phase reentry occurs in the region $\omega L/c \sim 17$–22. Last, for

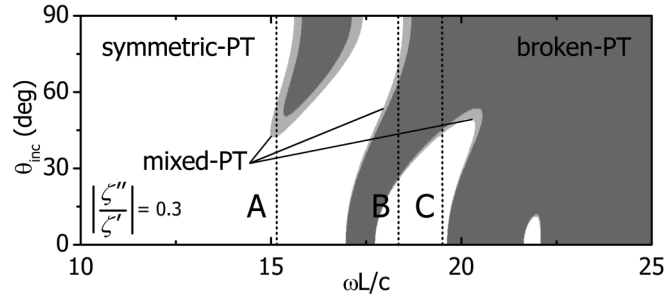

FIG. 5. Universal phase diagram for a system with $n = 2 \mp 0.1i$ and $|\zeta''/\zeta'| = 0.3$, corresponding to several choices for ε and μ. The possibilities for (a) mixed phases and (b) phase reentries can be achieved as function of either $\omega L/c$ or θ_{inc}, as denoted with the dashed vertical lines. The marked cases show partial phase reentry (line A), full phase reentry (line B), and typical phase change from *PT*-symmetric to the *PT*-broken phase (line C). Note that the cross section at $\theta_{inc} = 0$ corresponds to the plot shown in Fig. 4(b).

$\zeta'' = 1$ we observe several passes from the *PT*-symmetric to the broken-*PT* phase in the region $\omega L/c \sim 0$–16. At the same time, the exceptional points are shifted to lower $\omega L/c$, illustrating how their position can be further tailored via wave impedance engineering. The latter case ($\zeta_{g/l} = 1 \pm i$) maximizes the oscillation amplitude in the lhs of Eq. (6), because it corresponds to $\zeta' = \zeta''$, and therefore provides the maximum reentry effect. Additionally, $\zeta' = \zeta''$ corresponds to $\varphi = \pm\pi/4$ in accordance with our previous analysis and therefore the mixed phase is completely eliminated when we examine the same system in oblique incidence. In general, though, there is no need for such strict condition and both reentry effects and mixed phases can be still achieved if $|\zeta'|$, $|\zeta''|$ are not equal, especially at large angles where the $\cos\vartheta_{g/l}$ terms become significant. This will become apparent in the following example. In any case, the important conclusion is that, for a fixed refractive index $n_{g/l}$, all tunability depends on the ratio $|\zeta''/\zeta'|$ and not on the magnitude of ζ; the same phase diagrams correspond to any wave impedance with the same relative strength between its real and imaginary part. In other words, these graphs show a parametric family, which can be achieved with several different sets of ε and μ.

The results shown so far in terms of the normalized parameter $\omega L/c$ imply constant material parameters, which are not easily realizable with real, dispersive materials [21]. In practice, however, because the optical potential involves both the refractive index and the wave impedance—-besides the frequency—-, the *PT*-transition can be observed at a single frequency, with varying the values of gain and loss or just the incidence angle ϑ_{inc} (which tunes the angle $\vartheta_{g/l}$ that appears in $Z_{g/l}^{\text{TE}}$, $Z_{g/l}^{\text{TM}}$). To demonstrate this alternative, in Fig. 5 we show the phase diagram of the previous system with $n_g = 2$–$0.1i$, $n_l = 2 + 0.1i$, and $|\zeta''/\zeta'| = 0.3$ for $\vartheta_{inc} \neq 0$, i.e., we expand the case shown for normal incidence in Fig. 4(b) to account for oblique incidence.

This reveals a rich behavior and the possibilities for mixed phases and phase reentries as function of either $\omega L/c$ or ϑ_{inc}. The vertical dashed lines demonstrate three characteristic cases, which are accessible with scanning ϑ_{inc}, while keeping all the other parameters fixed. From this example it is evident

that partial phase reentries (line A), full phase reentries (line B), and typical phase changes (line C) are possible all within the same system with constant material parameters. Note also that in the examples shown in Fig. 4 and Fig. 5 we have assumed that $|\zeta''/\zeta'| \leqslant 1$. When the values of ζ'', ζ' are interchanged, this ratio is reversed, the TE and TM exceptional points exchange positions, and therefore the phase diagram remains the same (see Appendix for details).

III. INDEPENDENT CONTROL OF ANISOTROPIC TRANSMISSION RESONANCES

It is well known [16,18] that the scattering matrix can be alternatively defined to have its diagonal occupied by the transmission amplitudes, rather than the reflection amplitudes:

$$\begin{bmatrix} d \\ a \end{bmatrix} = S_c^p \begin{bmatrix} b \\ c \end{bmatrix} \equiv \begin{bmatrix} t^p & r_R^p \\ r_L^p & t^p \end{bmatrix} \begin{bmatrix} b \\ c \end{bmatrix}, \tag{7}$$

where the superscript $p = \{\mathrm{TE}, \mathrm{TM}\}$ denotes the respective polarization. This definition of S^p, which we will refer to as S_c^p in accordance with Ref. [18], results from simple permutation of the outgoing channels [compare with Eq. (2)] and therefore the eigenvalues of S^p and S_c^p are not the same. This fact naturally raises the question of whether the examined phase diagrams depend on the chosen representation.

As was shown in Refs. [18,23], while the exceptional points of S^p are associated with processes such as lasing or coherent perfect absorption, the exceptional points of S_c^p correspond to anisotropic transmission resonances (ATRs). These are points of operation where the reflectance from one side of the system is zero and the transmittance $T^p \equiv |t^p|^2$ is 100% from either side of the system (the eigenvalues of S_c^p are $\lambda_{c1,c2}^p = t^p \pm \sqrt{r_L^p r_R^p}$ and ATRs occur when $r_L^p = 0$ or $r_R^p = 0$ [18]). In the S_c^p representation, the PT-symmetric phase ($|\lambda_{c1}^p| = |\lambda_{c2}^p| = 1$) corresponds to $T^p < 1$ and the broken-PT phase ($|\lambda_{c1}^p| = 1/|\lambda_{c2}^p|$) to $T^p > 1$; in the mixed phase $T^p < 1$ for one polarization and $T^p > 1$ for the other. Hence, S^p and S_c^p describe different aspects of the same scattering process and the information provided by each one of them is unique and complementary.

As an example, in Fig. 6 we examine a system with $n_g = 2\text{–}0.1i$, $n_l = 2 + 0.1i$ and $\zeta_g = 1 + 0.3i$, $\zeta_l = 1\text{–}0.3i$, which falls under the general case of $|\zeta''/\zeta'| = 0.3$, previously examined in Fig. 5. In Fig. 6(a) we plot the phase diagram of S_c^p; the white background corresponds to the symmetric-PT phase for both polarizations, i.e., $|\lambda_{c1,c2}^{\mathrm{TE}}| = |\lambda_{c1,c2}^{\mathrm{TM}}| = 1$ and therefore $T^{\mathrm{TE}} < 1$ and $T^{\mathrm{TM}} < 1$. We denote the individual broken-PT phase for TE and TM waves as "$T^{\mathrm{TE}} > 1$" (magenta regions, where $|\lambda_{c1}^{\mathrm{TE}}| = 1/|\lambda_{c2}^{\mathrm{TE}}|$) and "$T^{\mathrm{TM}} > 1$" (striped regions where $|\lambda_{c1}^{\mathrm{TM}}| = 1/|\lambda_{c2}^{\mathrm{TM}}|$), respectively, and mixed phases occur where one of these regions overlaps with the white background (both regions overlapping leads to fully broken PT symmetry). The boundary of each region defines ATRs for each individual polarization. Whenever these individual boundaries cross, the ATRs coincide and TE and TM waves undergo simultaneously unidirectional reflectionless perfect transmission. Hence, these special points serve as ATRs for unpolarized light (marked here with open circles and denoted as "common ATR"). All other ATRs located at the boundaries of the individual regions occur for either TE or TM waves; these could serve as ATRs for polarization discrimination, for example. To further elucidate these aspects we choose $\vartheta_{inc} = 61.8^\circ$, where a common ATR occurs at $\omega L/c = 19.3$, and in Fig. 6(b) we show the calculated eigenvalues, in Fig. 6(c) the respective transmittances T^{TE} and T^{TM} and in Fig. 6(d) the reflectances R_R^{TE} and R_R^{TM}, where $R_R^p \equiv |r_R^p|^2$ (i.e., reflectances with wave incident from the right side).

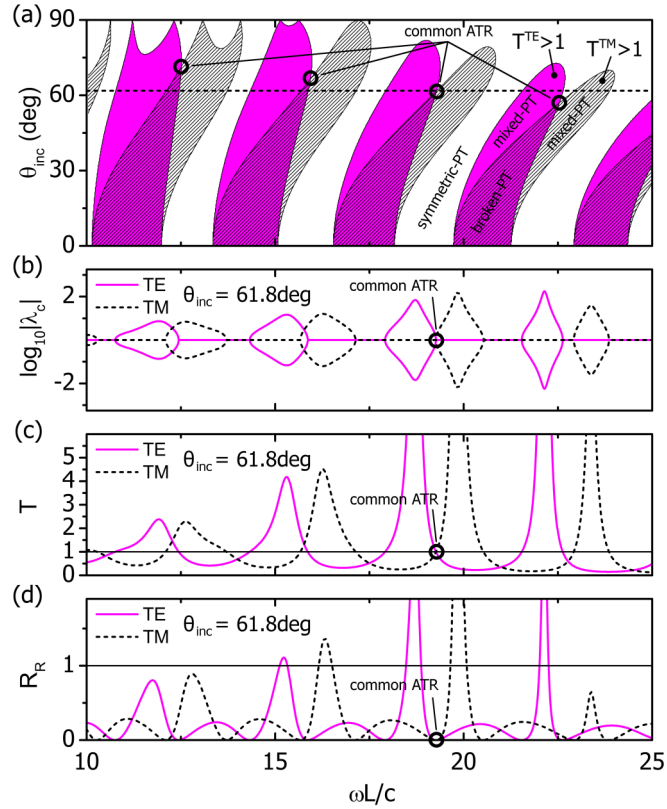

FIG. 6. System with $n = 2 \mp 0.1i$ and $\zeta = 1 \pm 0.3i$, examined in terms of S_c^p, the alternative definition for the scattering matrix. (a) Phase diagram. The white background denotes the simultaneous symmetric-PT phase of TE and TM waves; the magenta and striped regions correspond to the individual broken-PT phase of TE and TM waves, respectively. (b) Eigenvalues λ_c^{TE} and λ_c^{TM}, (c) transmittances T^{TE} and T^{TM}, and (d) reflectances R_R^{TE} and R_R^{TM}, at $\theta_{inc} = 61.8^\circ$. The common ATR points correspond to zero reflectance from one side of the system and 100% transmittance from either side, simultaneously for TE and TM waves.

In these plots it is evident that when the eigenvalues enter the broken-PT phase, the transmittance exceeds 100%. Exactly at the exceptional points the transmittance becomes 100% and the reflectance zero (ATR); for the chosen range we observe eight ATRs for TE waves and nine ATRs for TM waves in total. When two such points coincide (e.g., at $\omega L/c = 19.3$) an ATR common for both polarizations occurs.

Contrary to S^p, where the positions of the exceptional points do not depend on the magnitude of ζ but solely on the ratio $|\zeta''/\zeta'|$, in the case of S_c^p they do depend on the exact values of ζ', ζ''. As a result, while a certain $|\zeta''/\zeta'|$ ratio defines a unique phase diagram for S^p, it corresponds to multiple phase diagrams for S_c^p. This fact is of great importance, as it

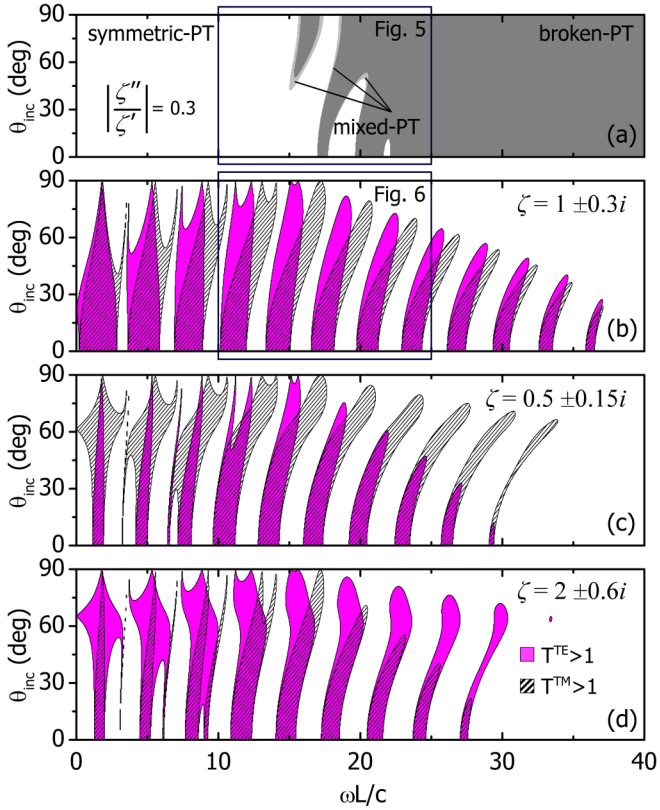

FIG. 7. Demonstration of independent control of S^p phases (associated with lasing and coherent absorption) and S_c^p phases (associated with ATRs) for systems with $n = 2 \mp 0.1i$ and $|\zeta''/\zeta'| = 0.3$. The universal phase diagram of S^p is shown in (a) and below individual phase diagrams of S_c^p are shown for (b) $\zeta = 1 \pm 0.3i$, (c) $\zeta = 0.5 \pm 0.15i$, and (d) $\zeta = 2 \pm 0.6i$. The phase diagram of S^p corresponds to all three cases of S_c^p that satisfy $|\zeta''/\zeta'| = 0.3$ and therefore different ATRs can be engineered for a certain lasing configuration. The regions in (a) and (b) within the box correspond to the data shown in Fig. 5 and Fig. 6(a), respectively.

allows us to design the position of the ATRs (related to the exceptional points of S_c^p) independently of the position of the lasing operation (related to the exceptional points of S^p).

In relevance to our last example, this means that for other choices of ζ', ζ'' all satisfying $|\zeta''/\zeta'| = 0.3$ and thus corresponding to the universal phase diagram of Fig. 5, we expect different phase diagrams for S_c^p and therefore different configurations of ATRs

To demonstrate this possibility, we return to our last example with $n_g = 2$–$0.1i$, $n_l = 2 + 0.1i$ and choose three different wave impedances satisfying $|\zeta''/\zeta'| = 0.3$. The common phase diagram for S^p is shown in Fig. 7(a) and is an extended version of Fig. 5 as denoted with the box. The phase diagram for S_c^p is shown individually for each case, namely for (b) $\zeta_g = 1 + 0.3i$, $\zeta_l = 1 - 0.3i$, (c) $\zeta_g = 0.5 + 0.15i$, $\zeta_l = 0.5 - 0.15i$,and (d) $\zeta_g = 2 + 0.6i$, $\zeta_l = 2 - 0.6i$. The color code follows the same conventions as in Fig. 6(a), which is repeated here in Fig. 7(b) to facilitate the comparison.

Clearly, for a certain $|\zeta''/\zeta'|$ ratio, the exact values of ζ', ζ'' change the phases of S_c^p and play no role in those of S^p. In other words, once the phase diagram of S^p is chosen, the phase diagram of S_c^p can be tuned independently. We emphasize here that with natural (nonmagnetic) materials the unique correspondence between n and ζ leads to a unique correspondence between the phase diagrams of S^p and S_c^p, and therefore no independent control between the individual exceptional points as we have demonstrated.

IV. CONCLUSION

In conclusion, we have shown that the coexistence of *PT*-symmetric, *PT*-broken, and mixed phases is possible even in simple one-dimensional photonic heterostructures with a single gain/loss bilayer. This plethora of phases including reentry behaviors (see Fig. 5) emerges as a result of the different wave impedances, properly engineered, between TE and TM linearly polarized waves; by varying the relative strength of these impedances simply through the angle of oblique incidence the obtained very rich phase diagram is achieved without requiring polarization converting elements or other additional components. We have further shown that the exceptional points of TE and TM waves can be tuned to modify and even suppress the mixed phase. We have also shown that, while natural materials favor a single exceptional point and thus a unique passing from *PT*-symmetric to *PT*-broken phase, with metamaterials it is possible to engineer the wave impedance (independently of the refractive index) to observe multiple exceptional points and therefore phase reentries. All the above possibilities become clear when the system is examined under the prism of n and ζ, rather than ε and μ. Specific cases examined in previous works all fall within our generalized approach, which provides a unified description, deep insight, and specific guidelines for the design of the desired response.

ACKNOWLEDGMENTS

This work was supported by the Hellenic Foundation for Research and Innovation (HFRI) and the General Secretariat for Research and Technology (GSRT), under the HFRI Ph.D. Fellowship grant (GA. No. 4820). It was also supported by the EU-Horizon2020 FET projects Ultrachiral and Visorsurf.

APPENDIX

1. Scattering amplitudes of TE and TM waves in oblique incidence

To find the reflection and transmission amplitudes of the double-slab system we solve Maxwell's equations with the boundary conditions at each material interface. We assume that waves arrive at angle ϑ_{inc} from either side of the system, with polarization which can be a mixture of TE components (H_x, E_y, H_z) and TM components (E_x, H_y, E_z) as shown in Fig. 1. For simplicity we assume that the surrounding space is air and, therefore the wave number outside the double slab is k_0, the free-space wave number. Inside each slab region the waves propagate at angle ϑ_i, (the subscript $i = \{g, l\}$ denotes the *gain* and *loss* region, respectively) and is given by $k_0 \sin(\vartheta_{inc}) = k_g \sin(\vartheta_g) = k_l \sin(\vartheta_l)$, which results from the continuity of the tangential field components at each interface. In the last relation $k_{g/l}$ is the wave number in each

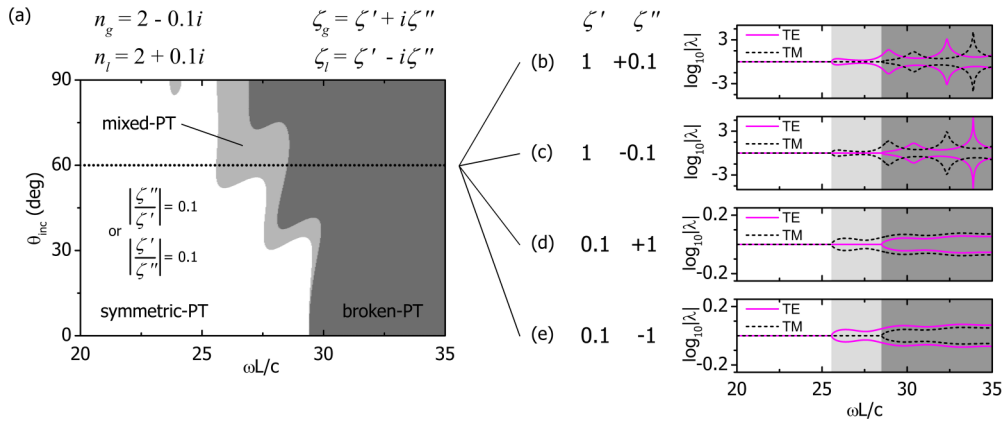

FIG. 8. Interchangeability of properties between TE and TM waves. (a) Universal phase diagram of the system of Fig. 4 with $n_{g/l} = 2 \mp 0.1i$ and $\zeta_{g/l} = \zeta' \pm i\zeta''$ with $\zeta' = 1$, $\zeta'' = \pm 0.1$ or $\zeta' = 0.1$, $\zeta'' = \pm 1$. Under these choices the range of the symmetric-*PT*, mixed-*PT*, and broken-*PT* phase is preserved. However, depending on the individual choice for ζ', ζ'', the magnitude of the eigenvalues changes, as shown on the right panels for $\vartheta_{inc} = 60^\circ$ and choice of (b) $\zeta' = 1$, $\zeta'' = +0.1$, (c) $\zeta' = 1$, $\zeta'' = -0.1$, (d) $\zeta' = 0.1$, $\zeta'' = +1$, and (e) $\zeta' = 0.1$, $\zeta'' = -1$. Notice how all choices share the same phase diagram, while the exceptional points of TE and TM waves may interchange positions. This general property owes its validity to the symmetric way that the wave impedances of TE and TM waves appear in Eq. (3).

region, which is given by $k_{g/l} = k_0\sqrt{\varepsilon_{g/l}\mu_{g/l}} \equiv k_0 n_{g/l}$, thereby reducing the relation to $\sin(\vartheta_{inc}) = n_{g/l}\sin(\vartheta_{g/l})$, as presented in the main text. To satisfy the *PT*-symmetry requirements given by Eq. (1), we are interested in material parameters of certain spatial symmetry; however, we start with slabs of arbitrary properties, ε_i, μ_i, and L_i, to obtain general expressions. The general (non-*PT*) analytical expressions for the reflection and transmission amplitudes, $r^p_{L/R}$ and $t^p_{L/R}$, are listed below. The subscript L/R denotes incidence from Left/Right and the superscript $p = \{\text{TE, TM}\}$ denotes the incident polarization.

TE polarization (H_x, E_y, H_z):

$$r_L^{\text{TE}} = -e^{-2iL_g k_0 \cos\theta_{inc}} \frac{C_L^{\text{TE}} + D_L^{\text{TE}}}{A^{\text{TE}} + B^{\text{TE}}}$$
$$r_R^{\text{TE}} = -e^{-2iL_l k_0 \cos\theta_{inc}} \frac{C_R^{\text{TE}} + D_R^{\text{TE}}}{A^{\text{TE}} + B^{\text{TE}}}$$

and $t_L^{\text{TE}} = t_R^{\text{TE}} \equiv t^{\text{TE}}$ with

$$t^{\text{TE}} = -8e^{-ik_0(L_g+L_l)\cos\theta_{inc}} e^{i(L_g k_g \cos\theta_g + L_l k_l \cos\theta_l)} \frac{R_g R_l \cos\theta_{inc}}{A^{\text{TE}} + B^{\text{TE}}}$$

TM polarization (E_x, H_y, E_z):

$$r_L^{\text{TM}} = -e^{-2iL_g k_0 \cos\theta_{inc}} \frac{C_L^{\text{TM}} + D_L^{\text{TM}}}{A^{\text{TM}} + B^{\text{TM}}}$$
$$r_R^{\text{TM}} = -e^{-2iL_l k_0 \cos\theta_{inc}} \frac{C_R^{\text{TM}} + D_R^{\text{TM}}}{A^{\text{TM}} + B^{\text{TM}}} \tag{A1}$$

and $t_L^{\text{TM}} = t_R^{\text{TM}} \equiv t^{\text{TM}}$ with

$$t^{\text{TM}} = -8e^{-ik_0(L_g+L_l)\cos\theta_{inc}} e^{i(L_g k_g \cos\theta_g + L_l k_l \cos\theta_l)} \frac{R_g R_l \cos\theta_{inc}}{A^{\text{TM}} + B^{\text{TM}}}$$

where $R_g = \frac{\cos\theta_g}{\cos\theta_{inc}}$ $R_l = \frac{\cos\theta_l}{\cos\theta_{inc}}$ and:

$$A^{\text{TE}} = Z_g\cos\theta_l\left(+\left(\tfrac{R_g}{Z_g}+1\right)+\left(\tfrac{R_g}{Z_g}-1\right)e^{2iL_g k_g\cos\theta_g}\right)\left(-\left(\tfrac{R_l}{Z_l}+1\right)+\left(\tfrac{R_l}{Z_l}-1\right)e^{2iL_l k_l\cos\theta_l}\right)$$
$$A^{\text{TM}} = Z_g\cos\theta_g\left(+\left(\tfrac{1}{Z_g}+R_g\right)+\left(\tfrac{1}{Z_g}-R_g\right)e^{2iL_g k_g\cos\theta_g}\right)\left(-\left(\tfrac{1}{Z_l}+R_l\right)+\left(\tfrac{1}{Z_l}-R_l\right)e^{2iL_l k_l\cos\theta_l}\right)$$

$$B^{\text{TE}} = Z_l\cos\theta_g\left(-\left(\tfrac{R_g}{Z_g}+1\right)+\left(\tfrac{R_g}{Z_g}-1\right)e^{2iL_g k_g\cos\theta_g}\right)\left(+\left(\tfrac{R_l}{Z_l}+1\right)+\left(\tfrac{R_l}{Z_l}-1\right)e^{2iL_l k_l\cos\theta_l}\right)$$
$$B^{\text{TM}} = Z_l\cos\theta_l\left(-\left(\tfrac{1}{Z_g}+R_g\right)+\left(\tfrac{1}{Z_g}-R_g\right)e^{2iL_g k_g\cos\theta_g}\right)\left(+\left(\tfrac{1}{Z_l}+R_l\right)+\left(\tfrac{1}{Z_l}-R_l\right)e^{2iL_l k_l\cos\theta_l}\right)$$

$$C_L^{\text{TE}} = Z_g\cos\theta_l\left(+\left(\tfrac{R_g}{Z_g}+1\right)e^{2iL_g k_g\cos\theta_g}+\left(\tfrac{R_g}{Z_g}-1\right)\right)\left(+\left(\tfrac{R_l}{Z_l}-1\right)e^{2iL_l k_l\cos\theta_l}-\left(\tfrac{R_l}{Z_l}+1\right)\right)$$
$$C_L^{\text{TM}} = Z_g\cos\theta_g\left(+\left(\tfrac{1}{Z_g}+R_g\right)e^{2iL_g k_g\cos\theta_g}+\left(\tfrac{1}{Z_g}-R_g\right)\right)\left(+\left(\tfrac{1}{Z_l}-R_l\right)e^{2iL_l k_l\cos\theta_l}-\left(\tfrac{1}{Z_l}+R_l\right)\right)$$

$$D_L^{\text{TE}} = Z_l\cos\theta_g\left(+\left(\tfrac{R_g}{Z_g}+1\right)e^{2iL_g k_g\cos\theta_g}-\left(\tfrac{R_g}{Z_g}-1\right)\right)\left(+\left(\tfrac{R_l}{Z_l}-1\right)e^{2iL_l k_l\cos\theta_l}+\left(\tfrac{R_l}{Z_l}+1\right)\right)$$
$$D_L^{\text{TM}} = Z_l\cos\theta_l\left(+\left(\tfrac{1}{Z_g}+R_g\right)e^{2iL_g k_g\cos\theta_g}-\left(\tfrac{1}{Z_g}-R_g\right)\right)\left(+\left(\tfrac{1}{Z_l}-R_l\right)e^{2iL_l k_l\cos\theta_l}+\left(\tfrac{1}{Z_l}+R_l\right)\right)$$

$$C_R^{\text{TE}} = Z_g\cos\theta_l\left(+\left(\tfrac{R_g}{Z_g}-1\right)e^{2iL_g k_g\cos\theta_g}+\left(\tfrac{R_g}{Z_g}+1\right)\right)\left(+\left(\tfrac{R_l}{Z_l}+1\right)e^{2iL_l k_l\cos\theta_l}-\left(\tfrac{R_l}{Z_l}-1\right)\right)$$
$$C_R^{\text{TM}} = Z_g\cos\theta_g\left(+\left(\tfrac{1}{Z_g}-R_g\right)e^{2iL_g k_g\cos\theta_g}+\left(\tfrac{1}{Z_g}+R_g\right)\right)\left(+\left(\tfrac{1}{Z_l}+R_l\right)e^{2iL_l k_l\cos\theta_l}-\left(\tfrac{1}{Z_l}-R_l\right)\right)$$

$$D_R^{\text{TE}} = Z_l\cos\theta_g\left(+\left(\tfrac{R_g}{Z_g}-1\right)e^{2iL_g k_g\cos\theta_g}-\left(\tfrac{R_g}{Z_g}+1\right)\right)\left(+\left(\tfrac{R_l}{Z_l}+1\right)e^{2iL_l k_l\cos\theta_l}+\left(\tfrac{R_l}{Z_l}-1\right)\right)$$
$$D_R^{\text{TM}} = Z_l\cos\theta_l\left(+\left(\tfrac{1}{Z_g}-R_g\right)e^{2iL_g k_g\cos\theta_g}-\left(\tfrac{1}{Z_g}+R_g\right)\right)\left(+\left(\tfrac{1}{Z_l}+R_l\right)e^{2iL_l k_l\cos\theta_l}+\left(\tfrac{1}{Z_l}-R_l\right)\right)$$

The parameter $Z_i = \sqrt{\mu_i/\varepsilon_i}$, $i = \{g, l\}$, is the wave impedance, which has been normalized to the free-space impedance $Z_0 = \sqrt{\mu_0/\varepsilon_0}$. For normal incidence, i.e., $\vartheta_{inc} = 0 \to \vartheta_g = \vartheta_l = 0$ and $R_g = R_l = 1$, $\cos\vartheta_g = \cos\vartheta_l = 1$. With simple substitution it is easy to verify that the scattering coefficients of the two polarizations become identical.

2. Condition for *PT*-symmetric phase and further examples

Previously, in order to clarify that the positions of the exceptional points for TE and TM waves do not depend on the magnitude of the wave impedance, but solely on the relative strength between its real and imaginary part, we expressed ζ_g and ζ_l in polar form. If, instead, we write the *PT*-symmetric

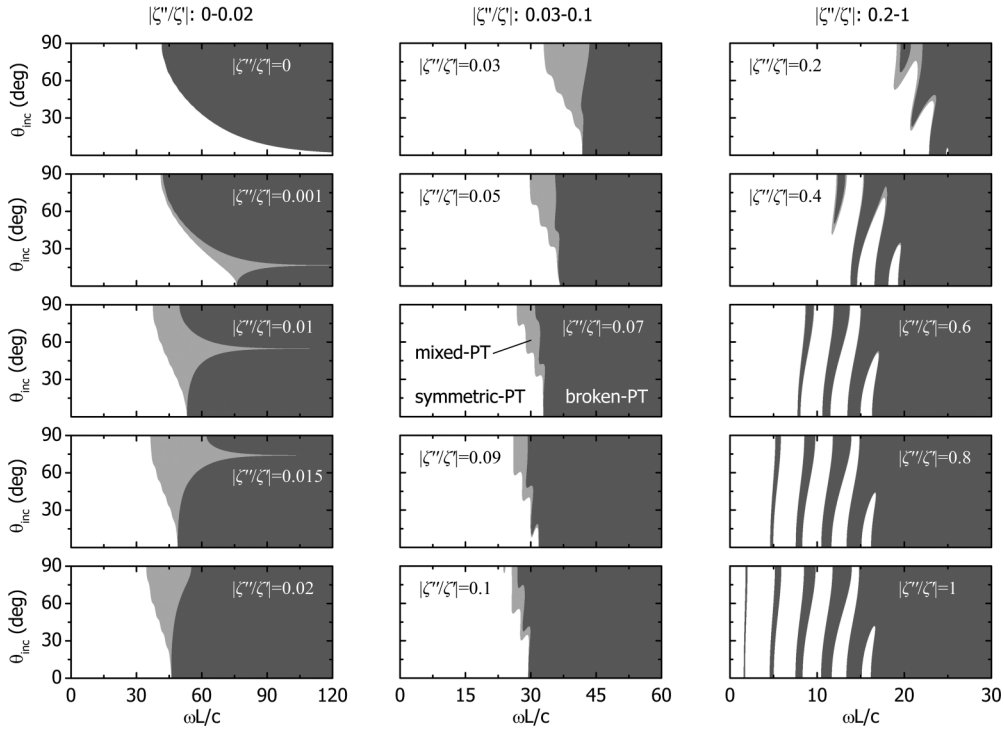

FIG. 9. Universal phase diagram and phase transformations. The system of Fig. 5 with $n = 2 \mp 0.1i$ is examined here, where the ratio $|\zeta''/\zeta'|$ is varied within the 0–1 range to demonstrate the phase transformations. Starting with $|\zeta''/\zeta'| = 0$, the mixed phase gradually appears with increasing $|\zeta''/\zeta'|$ and is subsequently suppressed until $|\zeta''/\zeta'| = 1$, where it is again eliminated. According to our previous analysis in terms of $\zeta_g = |\zeta|e^{+i\varphi}$ and $\zeta_l = |\zeta|e^{-i\varphi}$, the initial and final stages of this parametric study meet the condition that φ is multiple of $\pi/4$, leading the exceptional points of TE and TM waves to coincide and therefore the mixed phase to vanish.

ζ as $\zeta_{g/l} = \zeta' \pm i\zeta''$, ($\zeta'$,$\zeta''$: real quantities) then the criterion $|(r_L - r_R)/t| < 2$ for residing in the *PT*-symmetric phase as expressed in Eqs. (3a) and (3b) now takes the form

$$\text{TE}: \left|\left(\frac{\zeta' - i\zeta''}{\zeta' + i\zeta''}\frac{\cos\theta_g}{\cos\theta_l} - \frac{\zeta' + i\zeta''}{\zeta' - i\zeta''}\frac{\cos\theta_l}{\cos\theta_g}\right)\sin(\delta_g)\sin(\delta_l)\right| < 2$$
$$\text{TM}: \left|\left(\frac{\zeta' - i\zeta''}{\zeta' + i\zeta''}\frac{\cos\theta_l}{\cos\theta_g} - \frac{\zeta' + i\zeta''}{\zeta' - i\zeta''}\frac{\cos\theta_g}{\cos\theta_l}\right)\sin(\delta_g)\sin(\delta_l)\right| < 2. \quad \text{(A2)}$$

In this form it is easy to observe that, depending on the sign of ζ' and ζ'', the positions of the exceptional points either exchange between TE and TM waves or do not change at all. Simply put, the range of the *PT*-symmetric, mixed, and broken-*PT* phase remain the same regardless of the exact sign of ζ' and ζ'', which only defines which of the two polarizations crosses the EP first. Hence, all sign combinations for ζ',ζ'' that yield the same $|\zeta''/\zeta'|$ ratio fall under the same universal phase diagram. Additionally, with exchanging $\zeta' \leftrightarrow \zeta''$ the phase diagram is preserved, because we can restore the initial Eqs. (A2) by multiplying each wave impedance ζ by i. Hence, under the above transformations the positions of the exceptional points are immobile and a certain phase diagram may correspond to more than one wave impedance; however, the magnitude of the eigenvalues $\lambda^p_{1,2}$ changes in general within each broken-*PT* phase (in the symmetric-*PT* phase $|\lambda^p_{1,2}| = 1$, i.e., all eigenvalues have the same magnitude).

To demonstrate these conclusions, in Fig. 8 we return to the system of Figs. 4 and 5 with $n_g = 2 - 0.1i$ and $n_l = 2 + 0.1i$ and examine the cases with (a) $\zeta' = 1, \zeta'' = +0.1$, (b) $\zeta' = 1$, $\zeta = -0.1$, (c) $\zeta' = 0.1$, $\zeta'' = +1$, and (d) ζ' 0.1, $\zeta'' = -1$. These choices correspond to either $|\zeta''/\zeta'| = 0.1$ or $|\zeta'/\zeta''| = 0.1$ and provide therefore the same universal phase diagram, which is shown in Fig. 8(a). The eigenvalues for each case are shown in Figs. 8(b)–8(e) for $\vartheta_{inc} = 60^\circ$, as denoted with the dashed line in Fig. 8(a). Note that in all cases the magnitude of $\zeta_{g/l}$ is the same. Indeed, as we mentioned in Sec. II C, the positions of the exceptional points do not depend on the magnitude of ζ, but solely on the relative strength between its real and imaginary part.

Last, we examine how the mixed phases can be tuned with changing the relative strength of ζ', ζ''. In Fig. 9 we show the phase diagrams as the ratio $|\zeta''/\zeta'|$ increases from 0 to 1. For $|\zeta''/\zeta'| = 0$ the mixed phase is absent, but with

increasing $|\zeta''/\zeta'|$ ratio it gradually appears, then deforms to become subsequently suppressed until $|\zeta''/\zeta'| = 1$, where it is completely eliminated. According to our previous analysis in terms of $\zeta_g = |\zeta|e^{+i\varphi}$ and $\zeta_l = |\zeta|e^{-i\varphi}$, the initial and final stage of this parametric study meet the condition that φ is multiple of $\pi/4$, leading the exceptional points of TE and TM waves to coincide and therefore the mixed phase to vanish.

[1] C. M. Bender and S. Boettcher, Phys. Rev. Lett. **80**, 5243 (1998).
[2] C. M. Bender, S. Boettcher, and P. N. Meisinger, J. Math. Phys. **40**, 2201 (1999).
[3] C. M. Bender, D. C. Brody, and H. F. Jones, Phys. Rev. Lett. **89**, 270401 (2002).
[4] C. M. Bender, Rep. Prog. Phys. **70**, 947 (2007).
[5] R. El-Ganainy, K. G. Makris, D. N. Christodoulides, and Z. H. Musslimani, Opt. Lett. **32**, 2632 (2007).
[6] K. G. Makris, R. El-Ganainy, D. N. Christodoulides, and Z. H. Musslimani, Phys. Rev. Lett. **100**, 103904 (2008).
[7] S. Klaiman, U. Günther, and N. Moiseyev, Phys. Rev. Lett. **101**, 080402 (2008).
[8] A. Guo, G. J. Salamo, D. Duchesne, R. Morandotti, M. Volatier-Ravat, V. Aimez, G. A. Siviloglou, and D. N. Christodoulides, Phys. Rev. Lett. **103**, 093902 (2009).
[9] E. Rüter, K.G. Makris, R. El-Ganainy, D. N. Christodoulides, M. Sagev, and D. Kip, Nat. Phys. **6**, 192 (2010).
[10] Z. Lin, H. Ramezani, T. Eichelkraut, T. Kottos, H. Cao, and D. N. Christodoulides, Phys. Rev. Lett. **106**, 213901 (2011).
[11] L. Feng, Y. L. Xu, W. S. Fegadolli, M. H. Lu, J. E. Oliveira, V. R. Almeida, Y. F. Chen, and A. Scherer, Nat. Mater. **12**, 108 (2013).
[12] Y. Shen, X. Hua Deng, and L. Chen, Opt. Express **22**, 19440 (2014).
[13] Y. D. Chong, Li Ge, Hui Cao, and A. D. Stone, Phys. Rev. Lett. **105**, 053901 (2010).
[14] Y. Sun, W. Tan, H.Q. Li, J. Li, and H. Chen, Phys. Rev. Lett. **112**, 143903 (2014).
[15] S. Longhi, Phys. Rev. A **82**, 031801(R) (2010).
[16] Y. D. Chong, L. Ge, and A. D. Stone, Phys. Rev. Lett. **106**, 093902 (2011).
[17] Li Ge, Y. D. Chong, S. Rotter, H. E. Türeci, and A. D. Stone, Phys. Rev. A **84**, 023820 (2011).
[18] Li Ge, Y. D. Chong, and A. D. Stone, Phys. Rev. A **85**, 023802 (2012).
[19] N. Lazarides and G. P. Tsironis, Phys. Rev. Lett. **110**, 053901 (2013).
[20] J. M. Lee, S. Factor, Z. Lin, I. Vitebskiy, F. M. Ellis, and T. Kottos, Phys. Rev. Lett. **112**, 253902 (2014).
[21] A. A. Zyablovsky, A. P. Vinogradov, A. A. Pukhov, A. V. Dorofeenko, and A. A. Lisyansky, Phys. -Usp **57**, 1063 (2014).
[22] G. Castaldi, S. Savoia, V. Galdi, A. Alu, and N. Engheta, Phys. Rev. Lett. **110**, 173901 (2013).
[23] S. Droulias, I. Katsantonis, M. Kafesaki, C. M. Soukoulis, and E. N. Economou, Phys. Rev. Lett. **122**, 213201 (2019).
[24] S. Savoia, G. Castaldi, V. Galdi, A. Alu, and N. Engheta, Phys. Rev. B **89**, 085105 (2014).
[25] S. Savoia, G. Castaldi, V. Galdi, A. Alu, and N. Engheta, Phys. Rev. B **91**, 115114 (2015).
[26] J. Wang, H. Y. Dong, C. W. Ling, C. T. Chan, and K. H. Fung, Phys. Rev. B **91**, 235410 (2015).
[27] O. V. Shramkova and G. P. Tsironis, J. Opt. **18**, 105101, (2016).
[28] C.M. Soukoulis and M. Wegener, Nat. Photonics **5**, 523 (2011).
[29] E. Özgün, A. E. Serebryannikov, E. Ozbay, and C. M. Soukoulis, Sci. Rep. **7**, 15504 (2017).
[30] A. Mostafazadeh and M. Sarisaman, Phys. Rev. A **91**, 043804 (2015).
[31] R.-P. Guo, L.-T. Wu, X.-W. Cao, and J. Chen, J. Opt. **18**, 025611 (2016).
[32] M. Sarisaman, Phys. Rev. A **95**, 013806 (2017).